HHS Public Access

Author manuscript

Oncogene. Author manuscript; available in PMC 2015 July 29.

Published in final edited form as:

Oncogene. 2015 January 29; 34(5): 611–620. doi:10.1038/onc.2013.603.

Alternative lengthening of telomeres (ALT) in cancer stem cells in vivo

Bojana Bojovic, **Ryan E. Booth**, **Yi Jin**, **Xiaofeng Zhou**, and **David L. Crowe***

University of Illinois Cancer Center, 801 S. Paulina Street, Room 530C, Chicago, IL 60612 USA, Tel: 312-996-9488, Fax: 312-413-1604

Abstract

Chromosome ends are protected by telomeres which prevent DNA damage response and degradation. Telomerase expression extends telomeres and inhibits DNA damage response. Telomeres are also maintained by the recombination based alternative lengthening pathway. Telomerase is believed to be the sole mechanism for telomere maintenance in epidermis. We show that basal cells in epidermis maintain telomeres both by telomerase and ALT mechanisms in vivo. ALT was detected in epidermal stem cells in Terc−/− mice, and normal human epidermal keratinocytes are also ALT positive. ALT pathway is suppressed in primary but not metastatic epidermal squamous cell carcinomas (SCC) in Terc+/+ mice. ALT pathway is expressed in stem and basal cells in epidermal SCC in Terc−/− mice, and some telomerase positive human SCC lines. Telomeres shorten dramatically in stem and basal cells in epidermal SCC in vivo. Telomere shortening is associated with telomeric DNA damage response and apoptosis in stem and basal cells. Stem cells were transformed in both primary and metastatic epidermal SCC. Genetic ablation of this small cell population resulted in significant tumor regression in vivo. We concluded that alternative lengthening of telomeres is important in epidermal homeostasis and tumorigenesis in vivo.

Keywords

DNA damage; metastasis; squamous cell carcinoma; basal cells; keratin 15

INTRODUCTION

Chromosome ends are protected by telomeres which prevent DNA damage response and degradation (for review see 1). Telomeres form a large duplex loop mediated by single strand invasion of a G rich overhang (2, 3). When telomeres become critically short the DNA damage response is engaged at chromosome ends (for review see 4). Telomeres shorten in cultured cells to a critical length which induces senescence or apoptosis (5). In

*Corresponding author: dlcrowe@uic.edu.

CONFLICT OF INTEREST

The authors declare no conflicts of interest.

Terc null mutant mice, short telomeres exhibit DNA damage response followed by chromosomal fusions, aneuploidy, and apoptosis (6, 7).

Cellular subpopulations can stabilize their telomeres and continue proliferation by upregulation of telomerase (8–10). Telomerase extends telomeres using its Terc RNA template (11, 12). Telomerase overexpression can inhibit telomeric DNA damage response and immortalize cultured cells. Given the positive effects of telomerase on telomere length and cellular proliferation, telomerase activity is commonly upregulated in cancer cell lines and primary tumors (13).

Telomerase negative immortal cells exhibited significant heterogeneity of telomere length, suggesting an alternative mechanism of telomere lengthening (14). This alternative lengthening of telomeres (ALT) is a recombination based mechanism associated with formation of ALT associated PML bodies (APB; 15). Replication products of this pathway such as circular C rich strands are present in ALT cells (16). However the role of ALT in telomerase positive cells such as epidermal stem cells has not been investigated.

Alterations in telomere length regulation have profound effects on stem cells in epidermis (17, 18). Stem cells have longer telomeres than proliferating populations found in epidermis (19). In mammalian epidermis, an important stem cell population resides in the adult hair follicle bulge (20, 21). These slowly cycling keratin 15+ cells respond to external stimuli by increased cell division and migration, and are capable of regenerating components of the epidermis (22–24). Loss of telomerase activity inhibited proliferation and mobilization of stem cells and impaired hair growth (25), while telomerase overexpression caused transition to anagen with robust hair growth (26, 27). Telomerase also is expressed in the basal layer of epidermis, and its overexpression in this tissue increases tumor formation (28, 29). We previously demonstrated that telomerase expression is inhibited during suprabasal differentiation of keratinocytes via formation of a repressor complex containing the retinoblastoma tumor suppressor and histone deacetylase at E2F transcription factor binding sites in the telomerase promoter (30). However, limited telomere shortening was observed in keratinocytes cultured to senescence suggesting an alternative maintenance mechanism (31, 32). We show for the first time that basal but not stem cells in epidermis utilize both telomerase and ALT pathways under physiologic conditions in vivo. Epidermal stem cells activate ALT in the absence of telomerase, and are critical components of epidermal carcinogenesis and metastasis.

RESULTS

To determine the effects of telomerase deficiency on epidermal carcinogenesis, we treated GFP;Terc−/− and GFP;Terc+/+ mice with twice weekly doses of topical DMBA. As shown in Fig. 1A,B, both Terc−/− and Terc+/+ mice developed primary epidermal SCC with a mean latency period of 21 weeks. There were no significant differences in the number of primary tumors in Terc−/− and Terc+/+ mice, and all histopathologic subtypes of primary SCC (well, moderate, and poor differentiation) were equally represented in both groups. Telomerase activity was detected in Terc+/+ SCC but not in Terc−/− SCC.

Despite similarities in phenotype between primary Terc−/− and Terc+/+ SCC, Terc−/− SCC cells exhibited increased DNA damage response at telomeres (Fig. 1C–E). Increased telomeric localization of 53BP1 also was observed in sorted K15+ stem cells from Terc−/− primary SCC compared to those from Terc+/+ SCC (Fig. 1F,G; 8% vs. 0.4%; P<0.02). Increased apoptosis was observed in K15+ stem cells from Terc−/− primary SCC compared to Terc+/+ SCC (Fig. 1H,I; 6% vs. 0.5%; P<0.03). GFP+ and GFP− cells in normal epidermis, primary SCC, and metastatic SCC were telomerase positive, while all Terc−/− cells did not express telomerase activity (Fig. 1J). These results indicate that stem cells in Terc−/− SCC exhibit increased telomeric DNA damage response and apoptosis.

To determine if telomeric DNA response resulted in telomere shortening, we analyzed relative telomere length in GFP+ stem cells and GFP- basal cells sorted from normal epidermis, G1 Terc−/− epidermis, Terc+/+ SCC, G1 and G3 Terc−/− SCC, and metastatic SCC in the K15-CrePR;GFP mouse. As shown in Fig. 2A, relative telomere length was longer in GFP+ stem cells compared to GFP− basal cells in normal epidermis (0.9 vs. 0.6; P<0.04). Relative telomere length was shorter in GFP+ and GFP− cells from Terc−/− epidermis (0.5 and 0.4; P<0.05). Relative telomere length also was shorter in Terc+/+ SCC compared to Terc+/+ epidermis (0.5; P<0.04), although there were no longer significant differences between GFP positive and negative cells. Relative telomere length was shorter in G1 and G3 Terc−/− SCC compared to Terc+/+ SCC (0.35 and 0.2; P<0.02). Relative telomere length in metastatic cells was shortest of all cell types analyzed (0.2; P<0.01), despite these cells being sorted from Terc+/+ tumors. We were unable to obtain sufficient GFP+ cells from Terc−/− metastatic SCC for telomere length analysis. These results indicate that stem cell telomeres shorten during SCC tumorigenesis.

To determine if telomere single strand overhangs shorten along with telomeres during tumorigenesis, we compared relative overhang length in Terc+/+ and Terc−/− SCC in mice and in normal human keratinocytes (NHEK), immortalized keratinocytes (HOK16B), and SCC lines. As shown in Fig. 2B, relative overhang length was 80% shorter in the immortalized keratinocyte line HOK16B compared to NHEK cells (P<0.002). Relative overhang length was 25% shorter in G1 Terc−/− compared to Terc+/+ SCC (P<0.03). Relative overhang length in human SCC lines was 50% shorter on average compared to NHEK cells (range 10% to 75%; P<0.01; Fig. 2C). These results indicate that shorter single strand overhang length correlates with shorter telomere lengths during SCC tumorigenesis.

Terc−/− SCC cells exhibited telomeric FISH signals, indicating telomere maintenance in the absence of telomerase activity. To determine if telomeres in Terc−/− SCC were maintained by recombination based mechanisms, we screened several mouse and human cell strains and lines for a recognized marker of this alternative lengthening of telomeres (ALT) pathway (i.e., ALT associated PML bodies or APBs). We used U2OS human osteosarcoma cells as the positive control which is a well characterized telomerase negative/ALT positive line. PML protein co-localized at telomeres in U2OS cells as determined by immunofluorescence microscopy (Fig. 3A). Surprisingly we detected APBs in both Terc+/+ and Terc−/− mouse SCC lines (Fig. 3B,C). To determine if APBs are found in Terc+/+ human cells we screened NHEK cells which have low level telomerase activity, immortalized telomerase positive HOK16B cells, and 7 SCC lines with high levels of telomerase activity. As shown in Fig.

3D–F, APBs were detected in NHEK, HOK16B, and human SCC lines. These results indicate that both APBs and telomerase activity are found in human and mouse keratinocytes and SCC lines.

To more rigorously test for ALT pathway in Terc+/+ and Terc−/− keratinocytes, we sorted GFP+ and GFP- basal cells from mouse normal epidermis, primary SCC, and metastatic SCC. Genomic DNA from these populations was subjected to analysis of telomeric circular DNA, a recognized marker of the ALT pathway. As shown in Fig. 4A, GFP+ cells from normal epidermis were negative for telomeric circular DNA. Surprisingly circular DNA was detected in telomerase positive GFP− basal cells. However in Terc−/− epidermis, low levels of circular DNA were detected in GFP+ cells. GFP− cells from Terc−/− epidermis exhibited 2 fold higher levels of circular DNA than GFP+ cells. Terc+/+ SCCs exhibited low levels of circular DNA in both GFP+ and GFP− cells. Terc−/− SCCs demonstrated 2–4 fold higher levels of circular DNA in both GFP+ and GFP− cells compared to Terc+/+ SCC. GFP+ cells from metastatic SCC exhibited low levels of circular DNA, but highest levels of circular DNA were detected in metastatic GFP− cells (4 fold higher than in GFP− cells from primary SCC). These results indicate that telomeric circular DNA is found in telomerase positive non-stem cell populations. However, loss of telomerase activity was associated with increased circular DNA levels in both stem and non-stem cell groups.

We also screened several human cell lines and strains for the presence of telomeric circular DNA. As shown in Fig. 4B, the telomerase negative cell line U2OS exhibited high levels of circular DNA. The human telomerase positive cancer cell lines SCC4 and SCC9 also contained circular DNA, although at levels 15–25% of that found in U2OS cells. Five other telomerase positive human SCC lines were negative for telomeric circular DNA, as was the immortalized telomerase positive HOK16B cell line. However, we detected circular DNA in NHEK cells which express low levels of telomerase activity at early passage. These results indicate that normal human keratinocytes and some SCC lines contain telomeric circular DNA.

To confirm if increased telomeric circular DNA levels correlated with telomerase inhibition, we amplified circular DNA from Terc+/+, Terc+/−, and Terc−/− GFP+ and GFP− cells from mouse SCC. GFP+ and GFP− cells from Terc+/− SCC exhibited 2 fold higher levels of telomeric circular DNA than those from Terc+/+ SCC ($P<0.03$; Fig. 4C). GFP+ and GFP− cells from Terc−/− SCC exhibited 4–5 fold higher levels of telomeric circular DNA than those from Terc+/+ SCC ($P<0.01$). We also amplified serial dilutions of synthetic 96mer telomere circles in control reactions to demonstrate the linearity of the assay (Fig. 4D). These results indicate that telomeric circular DNA levels increase with telomerase inhibition in stem and non-stem SCC cells.

As an additional test of telomeric recombination, we examined sister chromatid exchange using chromosome orientation-fluorescence in situ hybridization (CO-FISH). Co-localization of fluorescent signals is indicative of telomeric sister chromatid exchange (TSCE) in this analysis. TSCE was detected in telomerase negative U2OS cells, a well characterized control line for this assay (Fig. 5A). Surprisingly TSCE was detected in both Terc+/+ and Terc−/− mouse SCCs (Fig. 5B,C). We also screened NHEK, HOK16B, and

human SCC lines for TSCE. Both NHEK and HOK16B demonstrated low levels of TSCE (Fig. 5D,E). Short telomeres in human SCC lines prevented assessment of TSCE in these cells. These results indicate that TSCE occurs in telomerase positive and negative keratinocyte and SCC lines.

To determine if telomere dysfunction-induced apoptosis in GFP+ stem cells correlated with depletion of this population, we sorted these cells from GFP negative, GFP+ Terc+/+, GFP+ G1 Terc−/− epidermis or SCCs by flow cytometry. GFP+ cells were not detected in control mice (Fig. 6A). We detected 1.9% GFP+ cells in Terc+/+ compared to 1.4% GFP+ cells in Terc−/− epidermis ($P<0.05$; Fig. 6B,C). We detected 1.0% GFP+ cells in SCCs, although significant differences between Terc+/+ and Terc−/− groups were not observed likely due to DMBA induced apoptosis (Fig. 6D). GFP+ cells were localized by immunofluorescence microscopy in both primary and metastatic SCC (Fig. 6E,F). Metastatic SCC from Terc+/+ and Terc−/− mice is shown in Fig. 6G,H. The number of positive lymph nodes was significantly reduced in Terc−/− SCC (65% vs. 36%; $P<0.04$; Fig. 6I), which correlated with increased telomeric DNA damage response and our inability to obtain substantial numbers of GFP+ cells from Terc−/− metastatic SCC. To determine the tumorigenicity of primary Terc+/+ and Terc−/− GFP+ tumor cells, we injected 10^4 of these cells subcutaneously into nude mice. Terc+/+ GFP+ tumor cells consistently formed tumors in nude mice by 6 months (Fig. 6J) characterized as poorly differentiated SCC (Fig. 6K). However Terc−/− GFP+ tumor cells formed tumors only in 40% of injections ($P<0.01$) and GFP- tumor cells failed to form tumors in nude mice by 6 months. These results indicate that stem cells are depleted in Terc−/− epidermis and SCCs. K15+ stem cells are found in both primary and metastatic SCC, but Terc−/− K15+ tumor cells are less tumorigenic in nude mice.

Our results indicate that telomerase inhibition depletes K15+ stem cells in SCC, resulting in decreased metastasis. To ensure that the effect of K15+ cell depletion was not solely an artifact of the telomerase null mutant model, we employed an orthogonal method of depleting K15+ cells in SCC using K15CrePR;GFP mice which express the reverse tetracycline activator (rTA) protein to transgenic mice expressing diphtheria toxin A (DTA) under control of the tet operon. When doxycycline is added to the mouse water supply, binding of the antibiotic to rTA induces expression of DTA which produces death of GFP+ cells. Using this system, GFP+ cells in doxycycline treated SCC were reduced from 2.1% to 0.3% ($P<0.001$). Strikingly, 35% of doxycycline treated tumors underwent complete regression. The remaining tumors in doxycycline treated mice were significantly smaller than in control mice (125 mm^3 vs. 750 mm^3; $P<0.001$). High grade tumors were not found in the doxycycline treated group compared to 42% of control SCCs. Histopathologic analysis of control SCCs demonstrated moderate to poorly differentiated primary and metastatic tumors (Fig. 7A,B). In contrast, stem cell depleted primary and metastatic SCCs were well differentiated or completely terminally differentiated as shown in Fig. 7C,D. Stem cell depleted SCCs exhibited significantly reduced number of lymph node metastases compared to control tumors (19% vs. 68%; $P<0.003$). These results indicated that depletion of the minor GFP+ stem cell population has dramatic effects on the in vivo phenotype of SCC, including decreased metastasis seen in Terc−/− tumors.

To begin to determine the mechanisms of stem cell depletion on SCC tumorigenesis, we characterized the numbers of apoptotic and proliferating cells in doxycycline treated and control tumors. As shown in Fig. 7E,G the number of apoptotic cells in doxycycline treated tumors increased from 4% to 87% as determined by TUNEL analysis ($P<0.004$). The number of proliferating cells decreased from 37% to 11% in doxycycline treated tumors as determined by PCNA immunohistochemistry (Fig. 7F,H; $P<0.005$). These results indicate that stem cell depletion reduces the number of proliferating cells and increases cell death during SCC tumorigenesis, which are similar to the effects of telomerase inhibition in Terc −/− tumors.

DISCUSSION

A key finding of this study is alternative lengthening of telomeres in telomerase positive epidermal basal cells in vivo. ALT also is detected in K15+ stem cells in the absence of telomerase activity. Previous studies show divergent conclusions regarding telomere maintenance by telomerase and ALT. APBs are maintained when telomerase is overexpressed in ALT positive cells (33). Conversely, APB formation is repressed in fusions of ALT and telomerase positive cells. Telomerase elongates the shortest telomeres but telomere length remains heterogeneous. Another study also demonstrates that telomerase expression inhibits the ALT pathway (34). Our results demonstrate that while ALT pathway is active in normal human epidermal keratinocytes, this mechanism is repressed in telomerase positive immortalized keratinocytes. Stratified epithelial cells are likely capable of maintaining telomeres by both telomerase and ALT; when one pathway becomes dominant it may compete with the other mechanism by elongating more telomeres. This mechanism would obviate the need for feedback regulation of telomerase and ALT pathways.

Another important finding of our study is suppression of ALT pathway in stem and basal cells in telomerase positive primary epidermal SCC. However ALT pathway is detected in basal cells of telomerase positive metastatic SCC, which also exhibits severe telomere shortening. Additionally we detect ALT pathway in 2 of 7 human SCC lines. In agreement with our results, both short telomeres and activation of the ALT pathway in cancers are independently associated with negative prognosis in human cancers (35). A recent survey of over 6000 primary cancers demonstrates ALT pathway activation in 3.7% of cases (36). Our results also demonstrate that ALT pathway is detected in stem and basal cells in Terc−/− SCC. Despite telomerase and ALT activation in epidermal SCC in vivo, our results demonstrate dramatically shortened telomeres in these cancers. This finding is likely the result of telomere shortening due to excess cell divisions prior to telomerase or ALT activation. We also demonstrate DNA damage response at telomeres in Terc−/− epidermal SCC. Activation of nucleases in DNA damage response pathways may also result in telomere shortening (37). Our results demonstrate shortening of the single strand G rich telomeric overhang in Terc−/− epidermal SCC and human SCC lines. The single strand overhang normally represses telomeric fusions (38), therefore shorter overhangs may contribute to chromosomal instability and tumorigenicity resulting from telomere end joining.

Our study also shows that normal epidermal stem cells contribute to both primary and metastatic SCC in Terc+/+ and Terc−/− mice. Fewer metastatic lesions are observed in Terc −/− SCC and stem cells from these tumors are less tumorigenic in immunocompromised mice than those from Terc+/+ cancers, likely due to increased DNA damage response and apoptosis. Genetic ablation of this small population (1% of tumor cells) results in dramatic terminal differentiation and regression of epidermal SCC with reduced metastasis. Depletion of stem cells in this model is substantially greater than that resulting from telomerase inhibition, which likely explains additional anti-tumor effects. These results expand on a previous finding of tumor regression when β-catenin signaling is inhibited in basal cells of epidermal SCC (39). The results of our study suggest that the minor transformed stem cell population is a critical regulator of proliferation and differentiation in epidermal SCC. Our results also confirm a previous finding of long telomeres in epidermal stem cells (22), but differences in telomere length between stem and basal cells are dramatically decreased during carcinogenesis. This finding may result from increased stem cell divisions needed to replace apoptotic basal cells lost during epidermal tumorigenesis. Future studies will focus on the mechanisms by which the transformed epidermal stem cell population dramatically regulates the phenotype of epidermal SCC.

MATERIALS AND METHODS

Mouse Breeding and Procedures

To determine the effects of telomerase inhibition on K15 positive stem cells in Terc+/+ and Terc−/− mouse epidermis, we bred B6;SJL-Tg(Krt1-15-cre/PGR)22Cot/J;*Gt(ROSA)26Sor*$^{tm1(rtTA,EGFP)Nagy}$/J mice to B6.Cg-*Terc*^{tm1Rdp}/J animals (The Jackson Laboratory, Bar Harbor, ME). Mice were injected with 200 μg of the progesterone receptor antagonist RU486 to express GFP and the reverse tet activator in K15+ cells. Twenty GFP;Terc+/+ and GFP;Terc−/− mice were used for tumorigenesis experiments. To ablate K15+ cells, GFP+ mice were crossed with Tg(tetO-DTA) animals. Following RU486 injection, doxycycline administration activated diphtheria toxin A expression in K15+ cells, resulting in cell death. In skin carcinogenesis experiments, we topically applied 25 μg dimethylbenzanthracene in ethanol to mouse epidermis twice weekly. Control mice received ethanol vehicle only. The latency, number, and volume of tumors were recorded for each animal. Skin and tumors from 9 month old mice were fixed in 4% buffered formaldehyde.

Cell Culture

Human and mouse SCC lines, human immortalized keratinocytes HOK16B, and U2OS cells were cultured in Dulbecco's modified Eagle medium, 10% fetal bovine serum, 40 μg/ml gentamicin at 37° C in a humidified atmosphere of 5% CO_2. Normal human epidermal keratinocytes (NHEK) were cultured in keratinocyte growth medium according to manufacturer's recommendations (Lonza, Walkersville, MD).

Telomeric Repeat Amplification Protocol

The TRAP assay was performed as described previously (16). Cells were lysed in buffer containing 10 mM Tris-HCl, pH 7.5, 1 mM $MgCl_2$, 1 mM EGTA, 0.1 mM benzamidine, 5 mM β-mercaptoethanol, 0.5% 3-[(3-cholamidopropyl)dimethylammonio]-1-

propanesulfonate (CHAPS), and 10% glycerol. After a 30 minute incubation on ice, the lysate was centrifuged for 30 min at 12,000 x g and the supernatant was stored at −80° C. Protein concentrations were determined by the Bradford method using Bio-Rad protein dye reagent according to manufacturer's recommendations. Extracts were diluted in lysis buffer and 5 ng of protein was incubated with 0.1 μg each TS 5′-AATCCGTCGAGCAGAGTT -3′ and ACX 5′-GCGCGG[CTTACC]$_3$CTAACC -3′ primers. An internal control oligonucleotide 5′-CGTCGAGCAGAGTTAAAAGGCCGAGAAGCGAT -3′ used for the quantification of telomerase activity was amplified using TS and a return primer 5′-ATCGCTTCTCGGCCTTTT -3′. The reaction mixture contained 50 μM of each deoxynucleotide triphosphate and 5 μCi [α-^{32}P]dCTP in 20 mM Tris-HCl, pH 8.3, 1.5 mM $MgCl_2$, 63 mM KCl, 0.05% Tween 20, 1 mM EGTA, and 2.5 U Taq DNA polymerase (Roche Applied Sciences, Indianapolis, IN). Following a 30 min incubation at 30° C, samples were subjected to 30 cycles of PCR at 94° C for 30 sec, 50° C for 30 sec, and 72° C for 1 min. The PCR products were separated on 10% non-denaturing polyacrylamide gels using 0.5X Tris-borate-EDTA running buffer. Gels were dried and exposed to autoradiographic film at −80° C for 16 hours. Heat inactivated extracts were used as the negative control.

Fluorescence Activated Cell Sorting

Epidermal keratinocytes and SCCs were dissociated using dispase followed by trypsin, washed in PBS, and sorted for GFP expression by flow cytometry (Becton Dickinson, Franklin Lakes, NJ).

Fluorescence In Situ Hybridization, Immunofluorescence, and Immunohistochemistry

Fixed mouse skin and tumor tissue was dehydrated in ethanol, cleared in xylene, and embedded in paraffin. Sections were deparaffinized and stained with hematoxylin and eosin. For telomeric fluorescence in situ hybridization, deparaffinized tissue sections or sorted cells were denatured with Cy3 labeled telomeric peptide nucleic acid probe $(TTAGGG)_3$ in 70% formamide at 80° C for 10 minutes followed by overnight incubation at room temperature. After washing, sections and cells were blocked with 10% normal serum and incubated with anti-53BP1 antibody overnight at room temperature. To detect ALT associated PML bodies at telomeres, cells were incubated with anti-PML and TRF2 antibodies. To detect GFP expression, tissue sections were incubated with anti-GFP antibody. Cells and sections were incubated with secondary antibodies conjugated to fluorescein or rhodamine and visualized by fluorescence microscopy. For immunohistochemical analysis, sections were incubated with anti-PCNA followed by biotinylated secondary antibody and streptavidin conjugated horseradish peroxidase. Antigen-antibody complexes were detected by incubation with peroxide substrate solution containing aminoethylcarbazole chromogen. Data were analyzed by Student t test.

Cell Death Analysis

Epidermal cells and tumor tissue sections were incubated with terminal deoxynucleotidyl transferase and dUTP-fluorescein for 1 hour at 37^0 C according to manufacturer's recommendations (Roche Applied Sciences, Indianapolis, IN). After washing apoptotic cells were visualized by fluorescence microscopy following coverslipping with anti-fade

mounting medium containing DAPI. The percentage of fluorescent cells in 10 random high power fields was determined.

Telomere Length Analysis of Sorted Cells

We used a quantitative PCR method to measure average telomere length ratios as described previously (40). Telomeric primers were 5′-CGGTTTGTTTGGGTTTGGGTTTGGGTTTGGGTTTGGGTT -3′ and 5′-GGCTTGCCTTACCCTTACCCTTACCCTTACCCTTAACCCT -3′. Primers for the mouse acidic ribosomal phosphoprotein PO (36B4) gene were 5′-ACTGGTCTAGGACCCGAGAAG – 3′ and 5′-TCAATGGTGCCTCTGGAGATT- 3′. Each reaction for the telomere assay included 12.5 μl of Syber Green PCR master mix (Applied Biosystems, Foster City, CA), 300 nM of each primer and 20 ng of genomic DNA. Samples were amplified in triplicate with reaction conditions of 95° C for 10 min followed by 30 cycles at 95° C for 15 sec and 56° C for 1 min. For the 36B4 assay, reaction conditions were 95° C for 10 min followed by 35 cycles at 95° C for 15 sec, 52° C annealing for 20 sec, and extension at 72° C for 30 sec. The relative input amount of telomere PCR was divided by the relative input amount of the 36B4 PCR. PCR was performed three times for each sample and the average of these ratios was reported as the average telomere length ratio.

Single Strand Overhang Length Analysis

Duplicate 5 μg denatured or native genomic DNA samples were blotted to nylon membranes followed by hybridization to ^{32}P-end labeled telomeric probe $(CCCTAA)_4$ in 6X SSC, 1X Denhardt's solution, 0.5% SDS at 50° C for 16 hours. Blots were washed in 4X SCC for 30 minutes at room temperature and exposed to autoradiographic film at −80° C for 16 hours.

Telomeric Circular DNA Analysis

Telomeric C-circle analysis was performed as described previously (41). Genomic DNA was digested with *Hinf*I and *Rsa*I. Telomeric circular DNA was amplified with ϕ29 DNA polymerase in the absence of dCTP and blotted to nylon membranes. Synthetic 96mer telomeric circles were used in control amplifications. Blots were hybridized with ^{32}P labeled $(TTAGGG)_4$ probe overnight at 50° C. After washing in 4X SCC, blots were exposed to autoradiographic film for 16 hours at −80° C.

Chromosome Orientation-Fluorescence In Situ Hybridization

CO-FISH analysis was performed as described previously (42). Cells were incubated for 16 hours with 30 μM BrdU and 10 μM BrdC followed by 90 minute incubation with 0.2 μg/ml colcemid. Harvested cells were incubated in 60 mM KCl at room temperature for 30 minutes, fixed in 3:1 methanol:acetic acid, and spotted to glass slides. Cells were incubated with 0.5 mg/ml RNase A for 10 min at 37°C. Cells were incubated with 0.5 μg/ml Hoechst 33258 for 15 min at room temperature. Cells were UV irradiated for 30 min and incubated with 800 U exonuclease III for 10 minutes at room temperature. After washing, slides were dehydrated in ethanol and hybridized with TelG-Cy3 peptide nucleic acid probe in 70%

formamide followed by TelC-FITC probe. Slides were washed extensively and examined using confocal microscopy.

Tumorigenicity Experiments

10^2–10^4 GFP+ or GFP- cells from Terc+/+ or Terc−/− primary tumors were injected subcutaneously into 2 month old NU/J mice. Mice were examined weekly for tumor formation for up to 6 months. Tumor sections were stained with hematoxylin and eosin.

Acknowledgments

We thank Dr. Chiayeng Wang (University of Illinois, Chicago, IL) for U2OS cells.

This research was supported by National Institutes of Health grant DE14283.

References

1. Palm W, de Lange T. How shelterin protects mammalian telomeres. Ann Rev Genet. 2008; 42:301–334. [PubMed: 18680434]
2. Griffith JD, Comeau L, Rosenfield S, Stansel RM, Bianchi A, Moss H, de Lange T. Mammalian telomeres end in a large duplex loop. Cell. 1999; 97:503–514. [PubMed: 10338214]
3. Hemann MT, Greider CW. G strand overhangs on telomeres in telomerase deficient mouse cells. Nuc Acids Res. 1999; 27:3964–3969.
4. Martinez P, Blasco MA. Role of shelterin in cancer and aging. Aging Cell. 2010; 9:653–666. [PubMed: 20569239]
5. Counter CM, Avilion AA, LeFeuvre CE, Stewart NG, Greider CW, Harley CB, Bacchetti S. Telomere shortening associate with chromosome instability is arrested in immortal cells which express telomerase activity. EMBO J. 1992; 11:1921–1929. [PubMed: 1582420]
6. Blasco MA, Lee HW, Hande MP, Samper E, Lansdorp PM, DePinho RA, Greider CW. Telomere shortening and tumor formation by mouse cells lacking telomerase RNA. Cell. 1997; 91:25–34. [PubMed: 9335332]
7. Rajaraman S, Choi J, Cheung P, Beaudry V, Moore H, Artandi SE. Telomere uncapping in progenitor cells with critical telomere shortening is coupled to S phase progression in vivo. Proc Natl Acad Sci USA. 2007; 104:17747–17752. [PubMed: 17965232]
8. Belair CD, Yeager TR, Lopez PM, Reznikoff CA. Telomerase activity: a biomarker of cell proliferation, not malignant transformation. Proc Natl Acad Sci USA. 1997; 94:13677–13682. [PubMed: 9391085]
9. Bodnar AG, Ouellette M, Frolkis M, Holt SE, Chiu CP, Morin GB, et al. Extension of lifespan by introduction of telomerase into normal human cells. Science. 1998; 279:349–352. [PubMed: 9454332]
10. Counter CM, Hahn WC, Wei W, Caddle SD, Beijersbergen RL, Lansdorp PM, et al. Dissociation among in vitro telomerase activity, telomere maintenance, and cellular immortalization. Proc Natl Acad Sci USA. 1998; 95:14723–14728. [PubMed: 9843956]
11. Harrington L, Zhou W, McPhail T, Oulton R, Yeung DS, Mar V, et al. Human telomerase contains evolutionarily conserved catalytic and structural subunits. Genes Dev. 1997; 11:3109–3115. [PubMed: 9389643]
12. Meyerson M, Counter CM, Eaton EN, Ellisen LW, Steiner P, Caddle SD, et al. hEST2, the putative human telomerase catalytic subunit gene, is upregulated in tumor cells and during immortalization. Cell. 1997; 90:785–795. [PubMed: 9288757]
13. Ramakrishnan S, Eppendberger U, Mueller H, Shinkai Y, Narayanan R. Expression profile of the putative catalytic subunit of the telomerase gene. Cancer Res. 1998; 58:622–625. [PubMed: 9485011]

14. Henderson S, Allsopp R, Spector D, Wang SS, Harley C. In situ analysis of changes in telomere size during replicative aging and cell transformation. J Cell Biol. 1996; 134:1–12. [PubMed: 8698806]
15. Wu G, Jiang X, Lee WH, Chen PL. Assembly of functional ALT associated promyelocytic leukemia bodies requires Nijmegen Breakage Syndrome 1. Cancer Res. 2003; 63:2589–2595. [PubMed: 12750284]
16. Nabetani A, Ishikawa F. Unusual telomeric DNAs in human telomerase negative immortalized cells. Mol Cell Biol. 2009; 29:703–713. [PubMed: 19015236]
17. Rossi DJ, Jamieson CHM, Weissman IL. Stem cells and the pathways to aging and cancer. Cell. 2008; 132:681–696. [PubMed: 18295583]
18. Fuchs E. The tortoise and the hair: slow cycling cells in the stem cell race. Cell. 2009; 137:811–819. [PubMed: 19490891]
19. Flores I, Canela A, Vera E, Tejera A, Cotsarelis G, Blasco MA. The longest telomeres: a general signature of adult stem cell compartments. Genes Dev. 2008; 22:654–667. [PubMed: 18283121]
20. Morris RJ, Liu Y, Marles L, Yang Z, Trempus C, Li S, et al. Capturing and profiling adult hair follicle stem cells. Nature Biotechnol. 2004; 22:411–417. [PubMed: 15024388]
21. Fuchs E. Scratching the surface of skin development. Nature. 2007; 445:834–842. [PubMed: 17314969]
22. Liu Y, Lyle S, Yang Z, Cotsarelis G. Keratin 15 promoter targets putative epithelial stem cells in the hair follicle bulge. J Invest Dermatol. 2003; 121:963–968. [PubMed: 14708593]
23. Cotsarelis G. Epithelial stem cells: a folliculocentric view. J Invest Dermatol. 2006; 126:1459–1468. [PubMed: 16778814]
24. Fuchs E. Skin stem cells: rising to the surface. J Cell Biol. 2008; 180:273–284. [PubMed: 18209104]
25. Flores I, Cayuela ML, Blasco MA. Effects of telomerase and telomere length on epidermal stem cell behavior. Science. 2005; 309:1253–1256. [PubMed: 16037417]
26. Sarin KY, Cheung P, Gilison D, Lee E, Tennen RI, Wang E, et al. Conditional telomerase induction causes proliferation of hair follicle stem cells. Nature. 2005; 436:1048–1052. [PubMed: 16107853]
27. Siegl-Cachedenier I, Flores I, Klatt P, Blasco MA. Telomerase reverses epidermal hair follicle stem cell defects and loss of long term survival associated with critically short telomeres. J Cell Biol. 2007; 179:277–290. [PubMed: 17954610]
28. Harle-Bachor C, Boukamp P. Telomerase activity in the regenerative basal layer of the epidermis in human skin and in immortal and carcinoma derived skin keratinocytes. Proc Natl Acad Sci USA. 1996; 93:6476–6481. [PubMed: 8692840]
29. Gonzalez-Suarez E, Samper E, Ramirez A, Flores JM, Martin-Caballero J, Jorcano JL, Blasco MA. Increased epidermal tumors and increased skin wound healing in transgenic mice overexpressing the catalytic subunit of telomerase mTERT in basal keratinocytes. EMBO J. 2001; 20:2619–2630. [PubMed: 11387197]
30. Crowe DL, Nguyen DC, Tsang KJ, Kyo S. E2F-1 represses transcription of the human telomerase reverse transcriptase gene. Nuc Acids Res. 2001; 29:2789–2794.
31. Kang MK, Guo W, Park NH. Replicative senescence of normal human oral keratinocytes is associated with the loss of telomerase activity without shortening of telomeres. Cell Growth Diff. 1998; 9:85–95. [PubMed: 9438392]
32. Kang MK, Kameta A, Shin KH, Baluda MA, Park NH. Senescence occurs with hTERT repression and limited telomere shortening in human oral keratinocytes cultured with feeder cells. J Cell Physiol. 2004; 199:364–370. [PubMed: 15095283]
33. Grobelny JV, Kulp-McEliece M, Broccoli D. Effects of reconstitution of telomerase activity on telomere maintenance by the alternative lengthening of telomeres (ALT) pathway. Hum Mol Genet. 2001; 10:1953–1961. [PubMed: 11555632]
34. Ford LP, Zou Y, Pongracz K, Gryaznov SM, Shay JW, Wright WE. Telomerase can inhibit the recombination based pathway of telomere maintenance in human cells. J Biol Chem. 2001; 276:32198–32203. [PubMed: 11395519]

35. Henson JD, Reddel RR. Assaying and investigating alternative lengthening of telomeres activity in human cells and cancers. FEBS Lett. 2010; 584:3800–3811. [PubMed: 20542034]
36. Heaphy CM, Subhawong AP, Hong SM, Goggins MG, Montgomery EA, Gabrielson E, et al. Prevalence of the alternative lengthening of telomeres telomere maintenance mechanism in human cancer subtypes. Am J Pathol. 2011; 179:1608–1615. [PubMed: 21888887]
37. Wu Y, Zacal NJ, Rainbow AJ, Zhu XD. XPF with mutations in its conserved nuclease domain is defective in DNA repair but functions in TRF2 mediated telomere shortening. DNA Repair. 2007; 6:157–166. [PubMed: 17055345]
38. van Steensel B, Smogorzewska A, de Lange T. TRF2 protects human telomeres from end to end fusions. Cell. 1998; 92:401–413. [PubMed: 9476899]
39. Malanchi I, Peinado H, Kassen D, Hussenet T, Metzger D, Chambon P, et al. Cutaneous cancer stem cell maintenance is dependent on β-catenin signaling. Nature. 2008; 452:650–653. [PubMed: 18385740]
40. Callicott RJ, Womack JE. Real time PCR assay for measurement of mouse telomeres. Comp Med. 2006; 56:17–22. [PubMed: 16521855]
41. Henson JD, Cao Y, Huschtscha LI, Chang AC, Au AYM, Pickett HA, Reddel RR. DNA C circles are specific and quantifiable markers of alternative lengthening of telomeres activity. Nature Biotechnol. 2009; 27:1181–1186. [PubMed: 19935656]
42. Celli GB, Lazzerini Denchi E, de Lange T. Ku70 stimulates fusion of dysfunctional telomeres yet protects chromosome ends from homologous recombination. Nature Cell Biol. 2006; 8:885–890. [PubMed: 16845382]

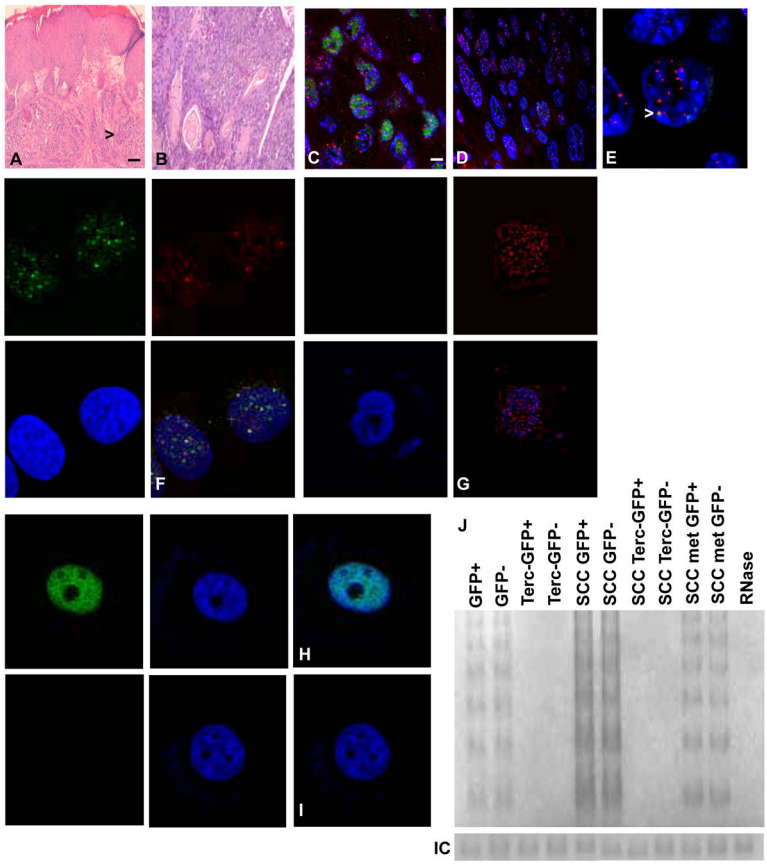

Fig. 1.

Terc−/− mice develop primary epidermal SCC. Tissue sections of primary SCC in Terc+/+ (A) and Terc−/− (B) mice are stained with hematoxylin and eosin. Arrows indicate tumor cells. Stem cells in Terc−/− mice exhibit telomeric DNA damage response and apoptosis. Localization of 53BP1 (FITC) at telomeres (Cy3) in tissue sections Terc−/− (C) and Terc+/+ (D) SCC is shown. Representative sections from three independent experiments are shown. Scale bar = 5 μm. (E) Enlarged photomicrograph showing localization of 53BP1 at telomeres (arrow) in Terc−/− SCC. Localization of 53BP1 protein at telomeres (yellow signals) in sorted stem cells from Terc−/− (F) and Terc+/+ (G) SCC. Apoptosis of sorted stem cells from Terc−/− (H) and Terc+/+ (I) SCC is shown by TUNEL analysis. (J) Telomerase activity in GFP+ and GFP- cells from normal epidermis, Terc negative epidermis, Terc+ and Terc- SCC, and metastatic SCC is shown by TRAP assay. RNase treated extract was used as the negative control.

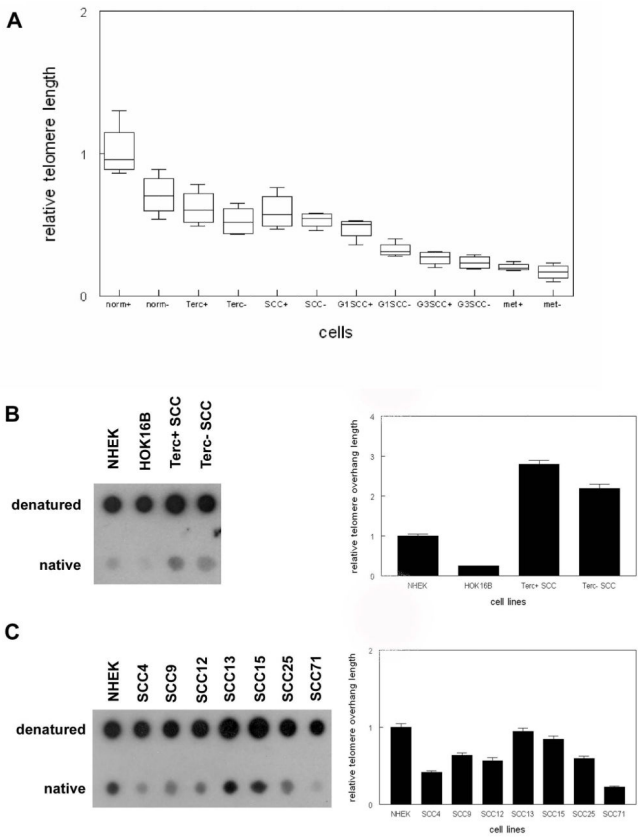

Fig. 2.

Shortening of telomeres and single strand overhangs in primary and metastatic epidermal SCC from Terc+/+ and Terc−/− mice. (A) Relative telomere length of sorted K15+ stem and basal (−) from wild type (norm), Terc−/−, Terc+/+ SCC, G1 Terc−/− SCC, G3 Terc−/− SCC, and Terc+/+ metastatic SCC was determined by qPCR as described in Materials and Methods. (B) Relative telomeric single strand overhang length in mouse Terc+/+ SCC, Terc −/− SCC, human NHEK, and HOK16B cells is shown by native and denatured southern blot. (C) Relative telomeric single strand overhang length in human NHEK and SCC lines is shown. A minimum of three independent experiments was performed. Representative blots are shown. Quantitation of blots is shown at right. Error bars indicate SEM.

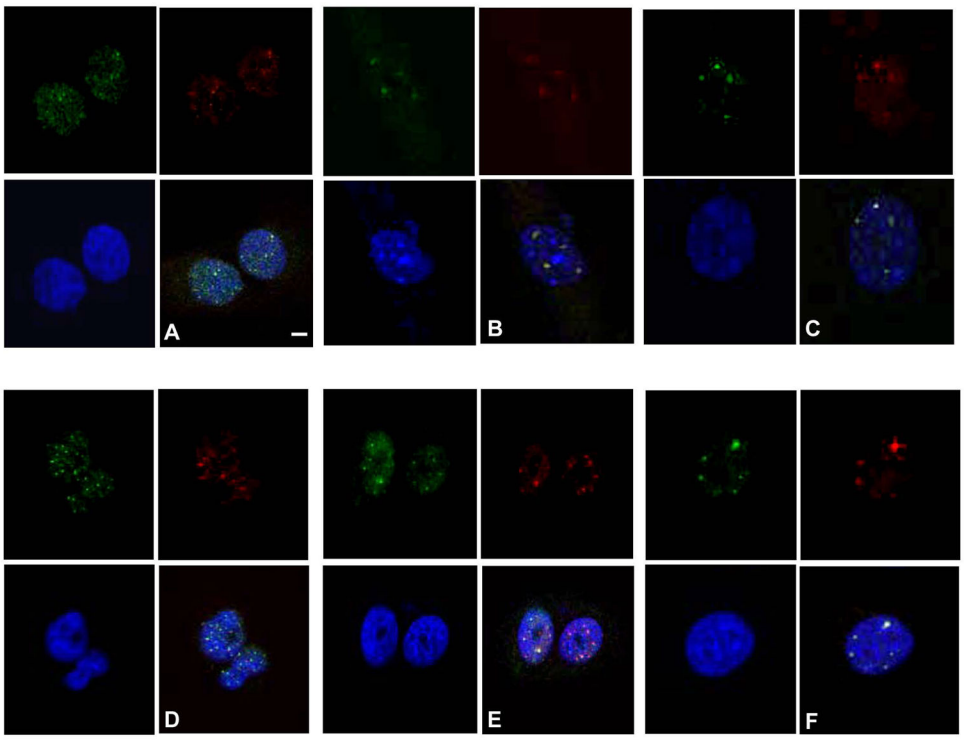

Fig. 3.

Terc+/+ keratinocytes and SCC exhibit ALT associated PML bodies. Colocalization of PML protein (FITC) and TRF2 (TRITC) is shown by double immunofluorescence in the U2OS cell line (A), Terc+/+ SCC (B), Terc−/− SCC (C), NHEK (D), HOK16B (E), and SCC4 cells (F). Nuclei were counterstained with DAPI. Scale bar = 2 μm. Representative photomicrographs from three independent experiments are shown.

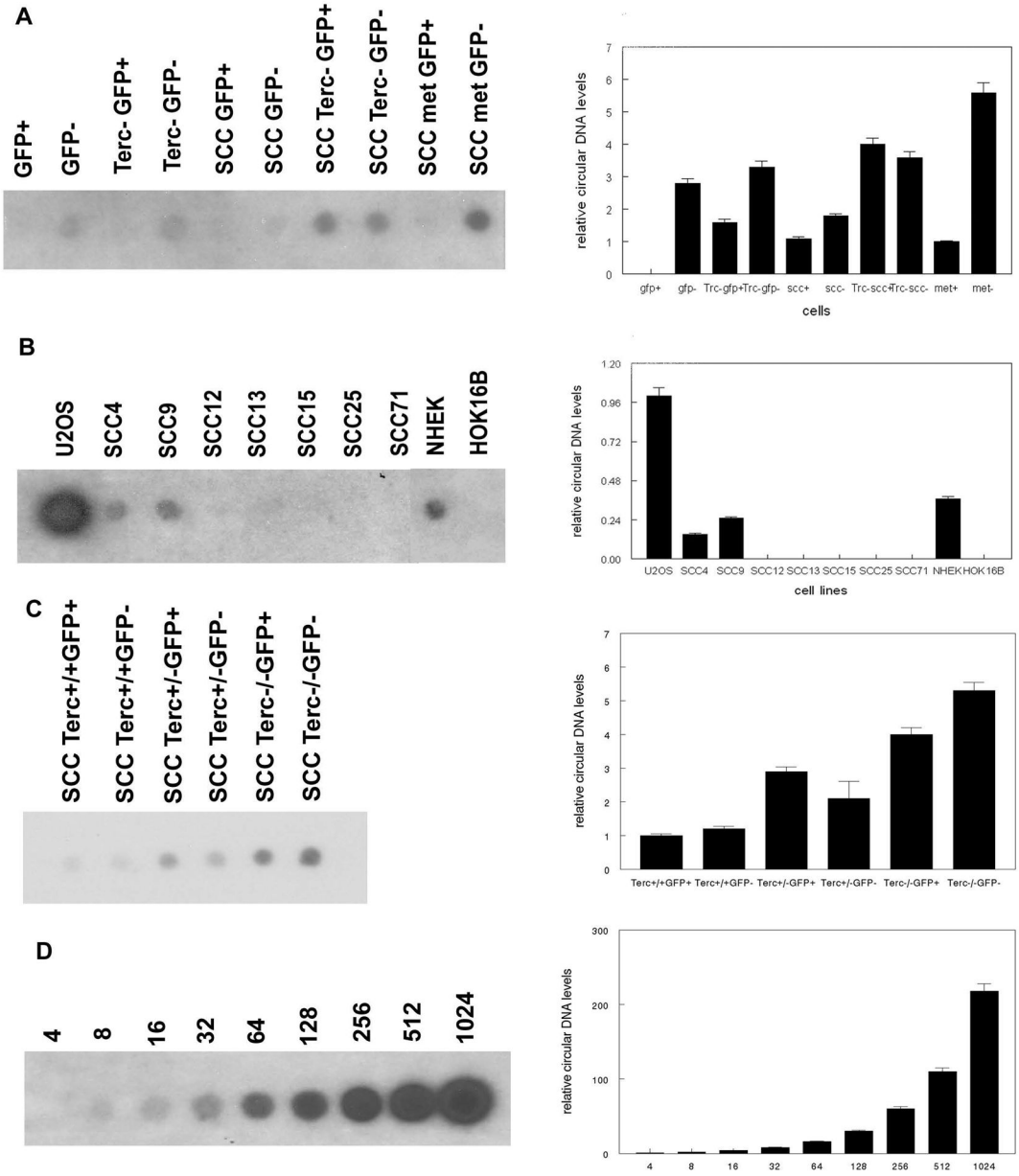

Fig. 4.

Terc+/+ keratinocytes and SCC exhibit telomeric circular DNA. (A) Telomeric circular DNA was amplified from mouse sorted Terc+/+ and Terc−/− epidermal stem (GFP+) and basal cells (GFP−), Terc+/+ and Terc−/− SCC cells, and Terc+/+ metastatic SCC cells and detected by southern blot. (B) Telomeric circular DNA was amplified from human U2OS, SCC, NHEK, and HOK16B cells. (C) Telomeric circular DNA was amplified in GFP+ and GFP− cells from Terc+/+, Terc+/−, and Terc−/− SCC. (D) Control amplifications of synthesized 96mer telomeric circular DNA. Nanograms of circular DNA in each reaction are shown. A minimum of three independent experiments was performed. Quantitation of blots is shown at right.

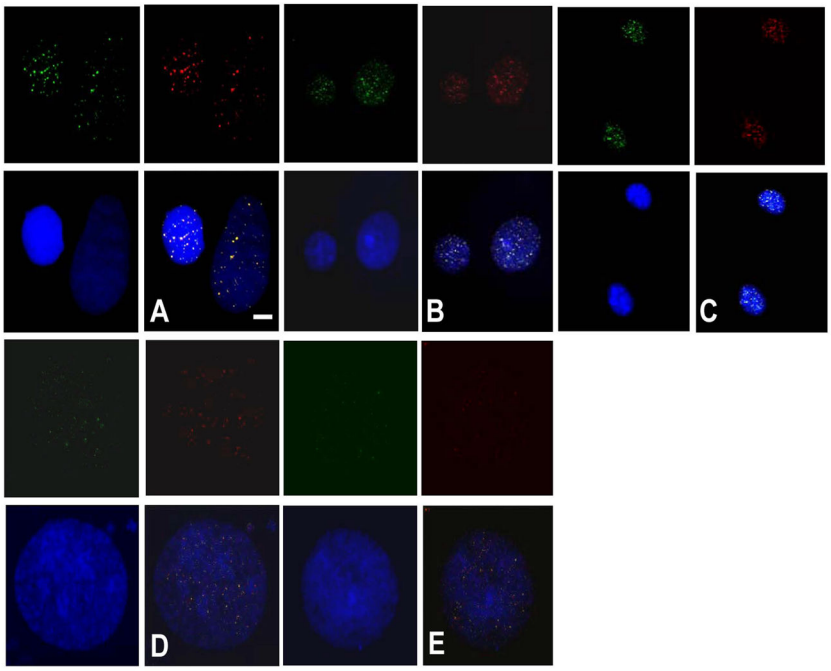

Fig. 5.

Terc+/+ keratinocytes and SCC exhibit recombination at telomeric sister chromatids. Chromosome orientation-fluorescent in situ hybridization was performed on human U2OS (A), mouse Terc+/+ SCC (B), mouse Terc−/− SCC (C), human NHEK (D), and human HOK16B (E) cells. Nuclei were counterstained with DAPI. Scale bar = 2 μm. A minimum of three independent experiments was performed. Representative photomicrographs are shown.

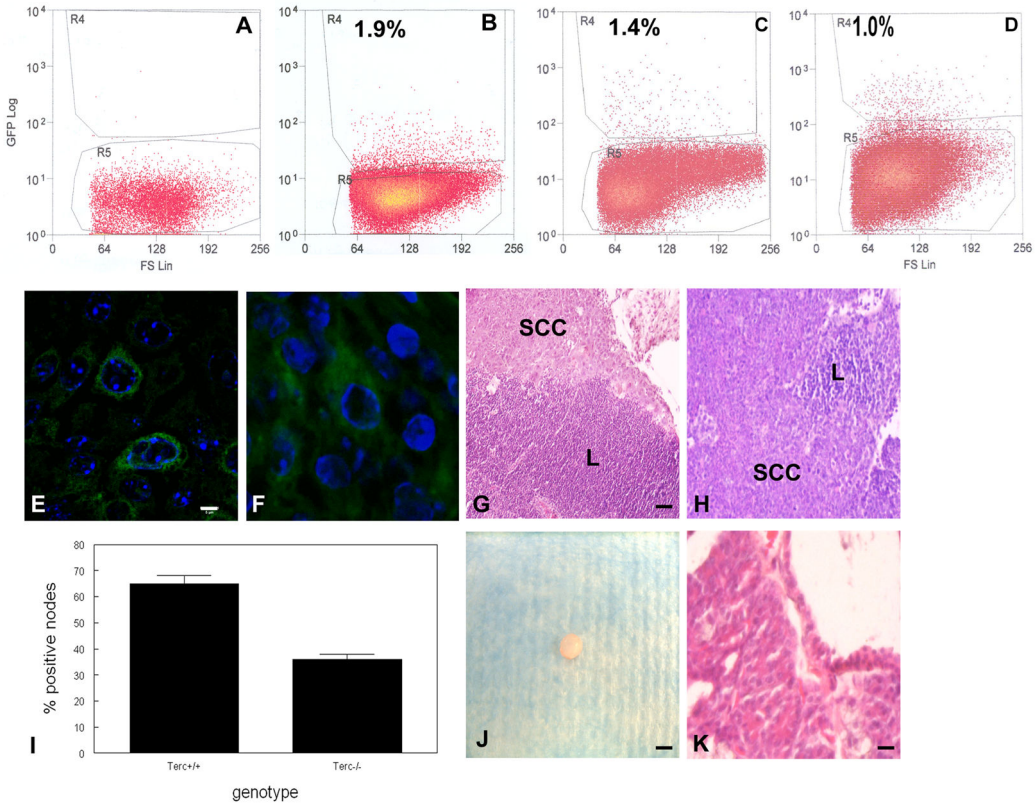

Fig. 6.

Stem cells from epidermal SCC are tumorigenic and contribute to primary and metastatic tumors. (A) Dissociated epidermal keratinocytes from control mice (A), K15/GFP/Terc+/+ mice (B), K15/GFP/Terc−/− mice (C), and K15/GFP epidermal SCC (D) were subjected to flow cytometric sorting. K15/GFP+ tumor cells were localized by immunofluorescence microscopy in primary (E) and metastatic (F) epidermal SCC. Scale bar = 2 μm. Metastatic SCC in Terc+/+ (G) and Terc−/− (H) mice is shown by hematoxylin and eosin staining. (I) Reduced metastatic SCC in Terc−/− compared to Terc+/+ SCC. (J) A tumor from sorted K15+ epidermal SCC cells subcutaneously injected into nude mice is shown. Scale bar = 5 mm. (K) A tissue section from tumor shown in (J) revealed poorly differentiated SCC. Scale bar = 50 μm.

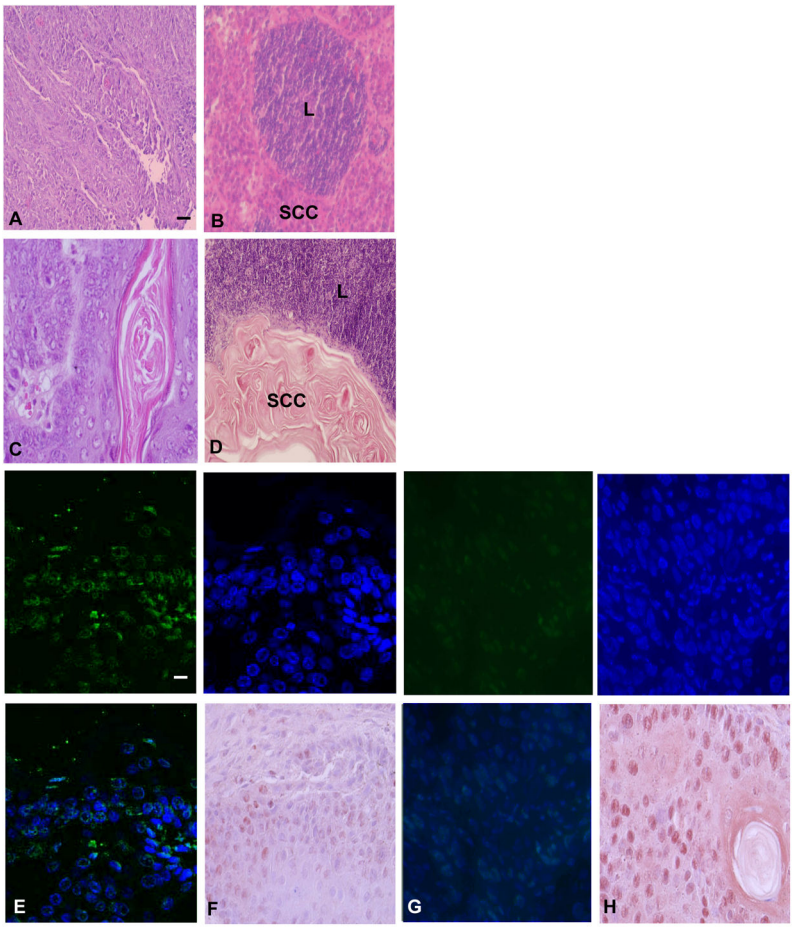

Fig. 7.

Regression of primary and metastatic SCC in K15+ stem cell depleted mice. Tissue sections of primary SCC in K15+ (A) and K15- (C) mice are shown stained with hematoxylin and eosin. Sections of metastatic SCC in regional lymph nodes of K15+ (B) and K15- (D) mice are shown. Both metastatic SCC and lymphocytes (L) are shown in representative sections. Scale bar = 50 μm. Increased apoptosis and reduced proliferation of tumor cells in K15- SCC. Apoptosis was measured by TUNEL analysis in tissue sections from K15- (E) and K15+ (G) SCC. Proliferation was measured by PCNA immunohistochemistry in K15- (F) and K15+ (H) SCC. A minimum of three independent experiments was performed. Representative sections are shown Scale bar = 10 μm.